Bifurcations in a Mathieu equation with cubic nonlinearities

Leslie Ng *, Richard Rand

Department of Theoretical and Applied Mechanics, Cornell University, Ithaca, NY 14853, USA

Accepted 11 October 2001

Abstract

We investigate the nonlinear dynamics of the classical Mathieu equation to which is added a nonlinearity which is a general cubic in x, $\dot{x}$. We use a perturbation method (averaging) which is valid in the neighborhood of 2:1 resonance, and in the limit of small forcing and small nonlinearity. By comparing the predictions of first-order averaging with the results of numerical integration, we show that it is necessary to go to second-order averaging in order to obtain the correct qualitative behavior. Analysis of the resulting slow-flow equations is accomplished both analytically as well as by use of the software AUTO. © 2002 Elsevier Science Ltd. All rights reserved.

1. Introduction

This work concerns the nonlinear differential equation

$$\frac{d^2x}{dt^2} + (\delta + \epsilon \cos t)x + \epsilon\left[Ax^3 + Bx^2\left(\frac{dx}{dt}\right) + Cx\left(\frac{dx}{dt}\right)^2 + D\left(\frac{dx}{dt}\right)^3\right] = 0 \tag{1}$$

The study of linear differential equations with periodic coefficients (Floquet theory) will not be able to produce a solution to Eq. (1), due to its nonlinearity. Nevertheless, Floquet theory may be used to determine the stability of the special solution $x = 0$, which is governed by Mathieu's equation, which is linear

$$\frac{d^2x}{dt^2} + (\delta + \epsilon \cos t)x = 0. \tag{2}$$

The transition curves separating regions of instability from those of stability for Eq. (2) are shown in Fig. 1.

Thus the question of the stability of the origin is the same for both the nonlinear equation (1) and the linear equation (2). However, because Eq. (1) is nonlinear, it may exhibit attractive periodic motions and even chaos, effects which are absent from the linear Mathieu equation (2).

Eq. (1) has been studied previously in two special cases: (i) $B = C = D = 0$ [3, p. 343] and (ii) $A = B = C = 0$ [3, p. 355]. We generalize these previous studies by investigating the nature of the solutions of Eq. (1) when all of the coefficients A, B, C, D are nonzero. Our approach is to use averaging to replace Eq. (1) by a slow flow, a step which is valid for small ϵ. We then investigate the bifurcations in the slow-flow equations.

Our interest in Eq. (1) comes from application to the dynamics of a cable being towed by a submarine [5]. Here the x^3 term comes from the approximation of $\sin x$ by $x - x^3/6$, corresponding to motions of moderate amplitude, and the $(dx/dt)^3$ term corresponds to nonlinear damping.

---

* Corresponding author.

E-mail address: lhn2@cornell.edu (L. Ng).
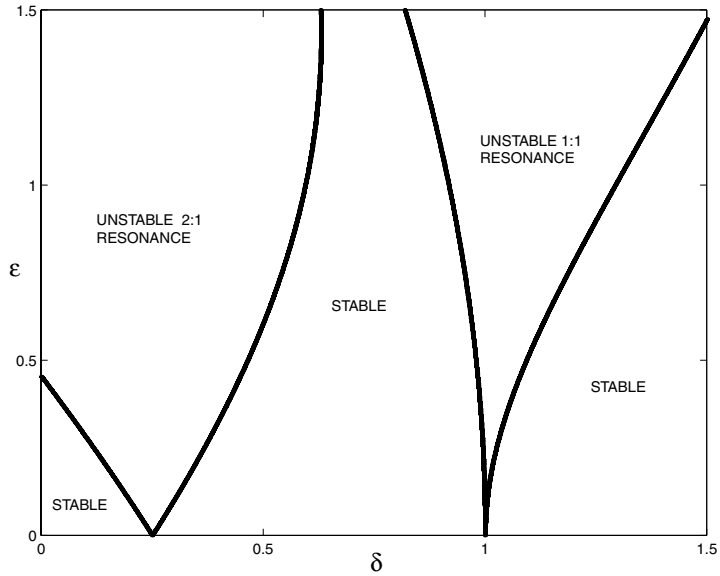
Fig. 1. Transition curves for the linear Mathieu equation.

2. Averaging

We set

$$\delta = \frac{1}{4} + \delta_1 \epsilon \tag{3}$$

in order to perturb off the well-known 2:1 resonance of the linear Mathieu equation. Then we set

$$x = R \cos \left(\frac{t}{2} + \psi \right) \quad \text{and} \quad \frac{\mathrm{d}x}{\mathrm{d}t} = -\frac{R}{2} \sin \left(\frac{t}{2} + \psi \right) \tag{4}$$

in which R and ψ are slowly varying functions of time t. Substituting Eq. (4) into Eq. (1) and averaging [6] over one cycle of duration 4π gives the slow-flow equations:

$$\frac{\mathrm{d}R}{\mathrm{d}t} = \epsilon \left(\frac{R}{2} \sin 2\psi - \beta R^3 \right), \tag{5}$$

$$\frac{\mathrm{d}\psi}{\mathrm{d}t} = \epsilon \left(\delta_1 + \frac{1}{2} \cos 2\psi + \alpha R^2 \right), \tag{6}$$

where

$$\alpha = \frac{3}{4} A + \frac{1}{16} C \quad \text{and} \quad \beta = \frac{1}{8} B + \frac{3}{32} D. \tag{7}$$

Equilibria in Eqs. (5) and (6) correspond to periodic motions in Eq. (1). These may be obtained by setting the right-hand sides of Eqs. (5) and (6) equal to zero, then solving the first for $\sin 2\psi$, and the second for $\cos 2\psi$, and then using the identity $\sin^2 2\psi + \cos^2 2\psi = 1$. This gives the following equation:

$$(\alpha^2 + \beta^2) R^4 + 2\alpha \delta_1 R^2 + \delta_1^2 - \frac{1}{4} = 0. \tag{8}$$

Eq. (8) is a quadratic on R^2, and may be easily solved. We find that in addition to the origin $R = 0$, there are additional slow-flow equilibria as follows, assuming $\alpha > 0$:

For $\delta_1 > \frac{1}{2}$, there are none.

For $-\frac{1}{2} < \delta_1 < \frac{1}{2}$, there is one.
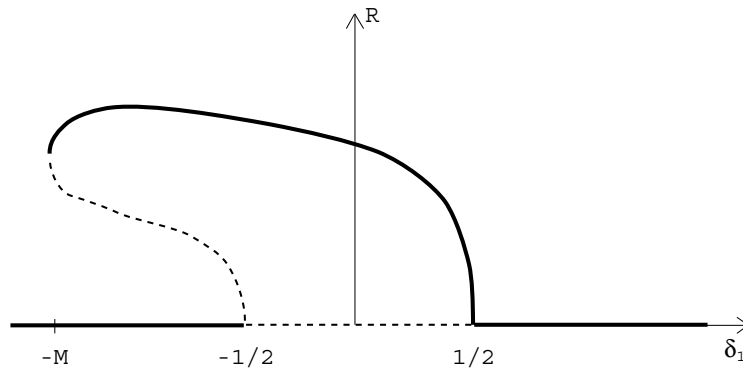
Fig. 2. Slow-flow equilibria for $\alpha > 0$.
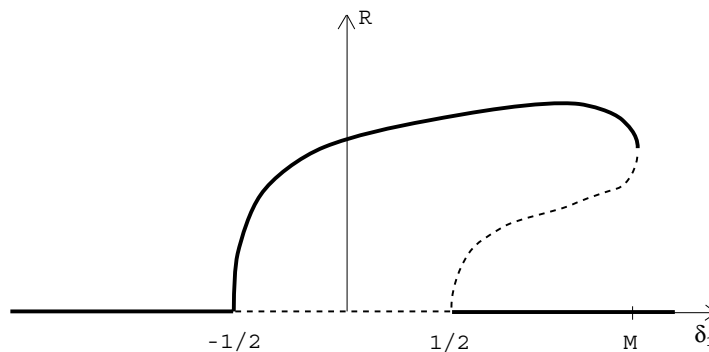
Fig. 3. Slow-flow equilibria for $\alpha < 0$.

For $-M < \delta_1 < -\frac{1}{2}$, there are two.

For $\delta_1 < -M$, there are none.

Here the quantity M turns out to be given by

$$M = \frac{1}{2}\sqrt{1 + \left(\frac{\alpha}{\beta}\right)^2} \tag{9}$$

This situation is illustrated in Fig. 2.

If $\alpha < 0$, however, the situation is reversed, as shown in Fig. 3. If we combine Figs. 2 and 3 for a fixed value of β, we get Fig. 4, which shows the number of (nonorigin) slow-flow equilibria in various regions of the δ–α parameter plane. Here ϵ has been fixed so that δ is given by Eq. (3). The curved lines in Fig. 4 are given by $\delta_1 = \pm M$.

3. Numerical integration

In order to test the validity of the foregoing analysis, we numerically integrated Eq. (1) for the following sample parameter values:

$$A = 1, \quad B = 3, \quad \delta_1 = 0.49, \quad \epsilon = 0.01, \quad \beta = \alpha. \tag{10}$$

We varied the remaining parameter, α, and obtained the Poincaré maps shown in Fig. 5. These maps are based on the surface of section $t = 0 \mod 2\pi$. The steady state periodic motions obtained in the averaging analysis would correspond to a period-2 motion in the Poincaré maps. This predicted motion is observed in Fig. 5(a). However, Figs. 5(b), (c) and (d) show dynamical features which are not predicted by the averaging analysis. In order to use averaging to explain these features, we found it necessary to extend the analysis to second-order averaging.
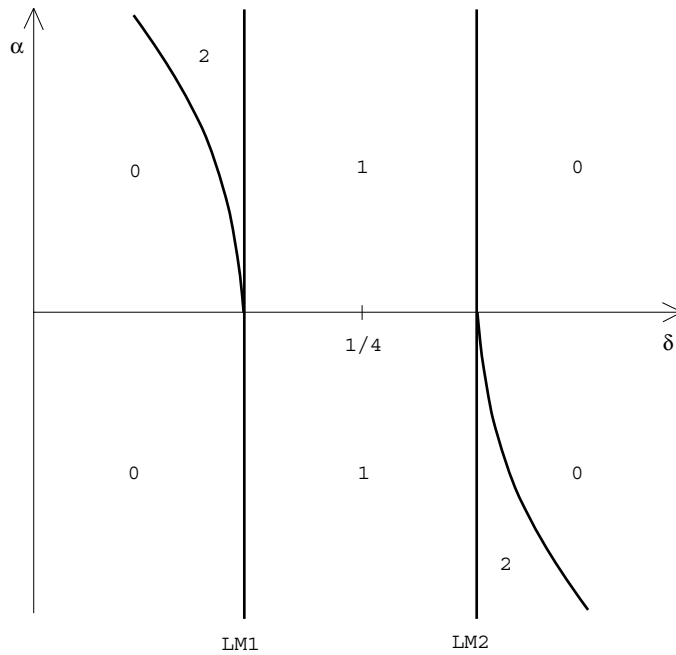
Fig. 4. Number of (nonorigin) slow-flow equilibria for β fixed as predicted by the first-order averaging.
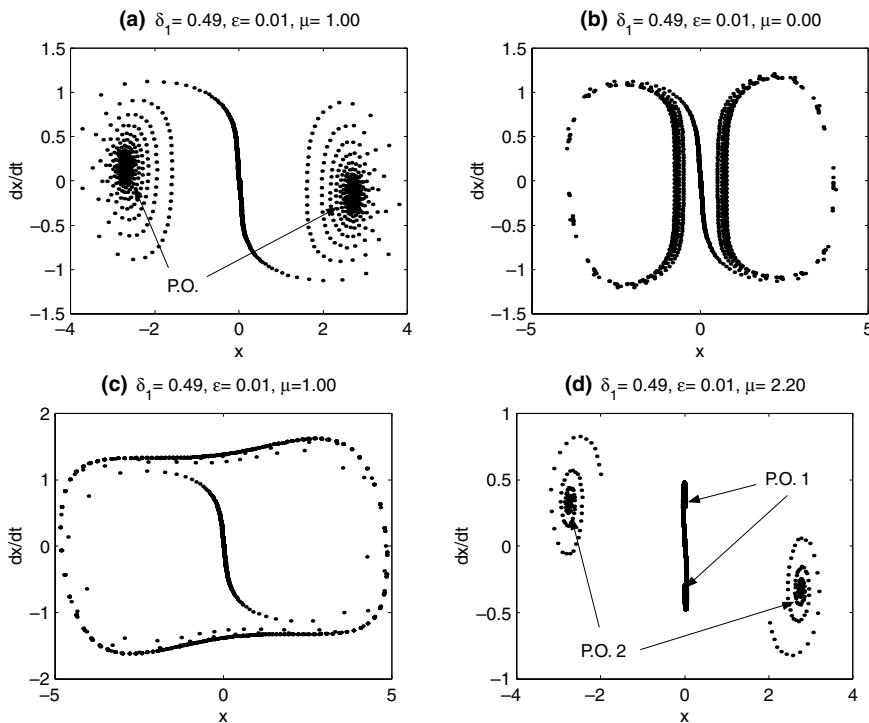
Fig. 5. Poincaré maps for $A = 1$, $B = 3$, $\epsilon = 0.01$, $\alpha = \beta = \epsilon\mu$ obtained by numerical integration of Eq. (1), arrows point to fixed points of the map (periodic orbits of Eq. (1)): (a) displays an attractive period-2 motion in the map which corresponds to a period 4π motion in Eq. (1); (b) and (c) displays quasi-periodic motions in Eq. (1); (d) displays bistability: two different sets of initial conditions are used which are attracted to two distinct period-2 motions.

4. Second-order averaging

To obtain a slow flow valid to $O(\epsilon^2)$, we follow the procedure in [4]. To accomplish this, we must expand the parameters δ, α and β to higher order in ϵ:

$$\delta = \frac{1}{4} + \delta_1\epsilon + \delta_2\epsilon^2, \tag{11}$$

$$\alpha = \alpha_0 + \alpha_1\epsilon \quad \text{and} \quad \beta = \beta_0 + \beta_1\epsilon. \tag{12}$$

We obtain the following slow-flow equations:

$$\frac{dR}{dt} = \epsilon\left(\frac{1}{2}R\sin 2\psi - \beta_0 R^3\right) + \epsilon^2\left(-\delta_1\sin 2\psi R + \left(-\frac{3}{2}\alpha_0\sin 2\psi + \frac{1}{2}A\sin 2\psi - \frac{7}{6}\beta_0\cos 2\psi\right.\right.$$
$$\left.\left. + \frac{1}{12}B\cos 2\psi - 2\beta_0\delta_1 + \frac{1}{2}B\delta_1 - \beta_1\right)R^3 + \left(\frac{4}{3}\alpha_0\beta_0 - 2A\beta_0 + \frac{1}{3}\alpha_0 B\right)R^5\right), \tag{13}$$

$$\frac{d\psi}{dt} = \epsilon\left(\delta_1 + \frac{1}{2}\cos 2\psi + \alpha_0 R^2\right) + \epsilon^2\left(-\delta_1\cos 2\psi + \delta_2 - \delta_1^2 - \frac{1}{8} + \left(\frac{1}{3}\beta_0\sin 2\psi + \frac{1}{3}B\sin 2\psi\right.\right.$$
$$\left.\left. + \alpha_0\cos 2\psi - 2A\cos 2\psi - 3A\delta_1 + \alpha_1\right)R^2 + \left(-\frac{3}{2}\beta_0^2 - \frac{1}{6}B\beta_0 - \frac{1}{24}B^2 - \frac{3}{2}\alpha_0^2 + A\alpha_0 - \frac{3}{2}A^2\right)R^4\right). \tag{14}$$

These equations are significantly more complicated than Eqs. (5) and (6). The fixed points of the system will now depend on the parameters δ_1, δ_2, ϵ, α_0, α_1, β_0, β_1, A and B. Because of the large number of parameters, several simplifications were made in order to make the analysis more tractable. First, we set α_0, $\beta_0 = 0$ since it will turn out that second-order averaging is most relevant when α and β are of $O(\epsilon)$. Second, we arbitrarily fix the parameters $A = 1$, $B = 3$ and set $\alpha_1 = \beta_1 = \mu$. These simplifications result in the following system:

$$\frac{dR}{dt} = \epsilon\left(\frac{1}{2}R\sin 2\psi\right) + \epsilon^2\left(-\delta_1 R\sin 2\psi + \left(\frac{3}{2}\delta_1 - \mu + \frac{1}{2}\sin 2\psi + \frac{1}{4}\cos 2\psi\right)R^3\right), \tag{15}$$

$$\frac{d\psi}{dt} = \epsilon\left(\delta_1 + \frac{1}{2}\cos 2\psi\right) + \epsilon^2\left(\delta_2 - \delta_1^2 - \frac{1}{8} - \delta_1\cos 2\psi + (\mu - 3\delta_1 + \sin 2\psi - 2\cos 2\psi)R^2 - \frac{15}{8}R^4\right). \tag{16}$$

The simplified slow-flow equations (15) and (16) now have a reduced parameter space of ϵ, μ, δ_1 and δ_2. If we regard ϵ as fixed but small and recall our previous assumption that $\delta = 1/4 + \epsilon\delta_1 + \epsilon^2\delta_2$, the perturbation $\delta = 1/4 + \epsilon\Delta$ gives $\Delta = \delta_1 + \epsilon\delta_2$. Thus, the system can be viewed in a 2-D parameter space of Δ and μ only. We will generally take $\delta_2 = 0$, since with ϵ fixed any value of Δ can be achieved by choosing $\Delta = \delta_1$. However, at points where δ_1 takes on critical values (i.e. where features change rapidly with δ_1), we will take δ_2 nonzero.

Performing a bifurcation analysis of Eqs. (15) and (16) includes finding the fixed points of the system, which requires solving a high-order polynomial in R. A combination of analytic and numerical techniques was used in this analysis. These included using Taylor series expansions at various stages of the calculation to produce approximate solutions and numerically solving the polynomial in R for different values of δ_1, δ_2, ϵ and μ and counting the number of positive real roots to determine the number of fixed points of the system. Fig. 6 (see Table 1) presents a bifurcation diagram summarizing the features observed for the simplified system equations (15) and (16) when $\epsilon = 0.01$.

The labels RI, RII, ... in Fig. 6 correspond to regions in parameter space with different numbers of fixed points. The remaining labels SN1, HO, ... identify various types of bifurcation curves.

The curves LM1 and LM2 represent bifurcations where a pair of saddle points along the $R = 0$ axis are created and destroyed. Analytic expressions for these curves can be obtained from Eq. (6). It was found that the equations for LM1 and LM2 are $\delta_1 = -1/2$, $\delta_2 = -1/8$ and $\delta_1 = +1/2$, $\delta_2 = -1/8$, respectively. These values correspond to the $O(\epsilon^2)$ expressions for the boundaries of the 2:1 resonance tongue present in the linear Mathieu equation.

The curves SN1, SN2, and SN3 correspond to saddle node bifurcations of Eqs. (15) and (16). Analytic approximations for SN1 and SN2 were obtained from Eqs. (15) and (16) using Taylor series expansions in ϵ. It was found that the equations

$$\delta_1 = \pm\frac{1}{2}, \quad \delta_2 = -\frac{1}{8} - \frac{2}{15}\left(\mu \pm \frac{1}{2}\right)^2, \quad \mu \pm \frac{1}{2} \geqslant 0 \tag{17}$$

approximate SN1, SN2, respectively, in the neighborhood of the LM1, LM2 curves.
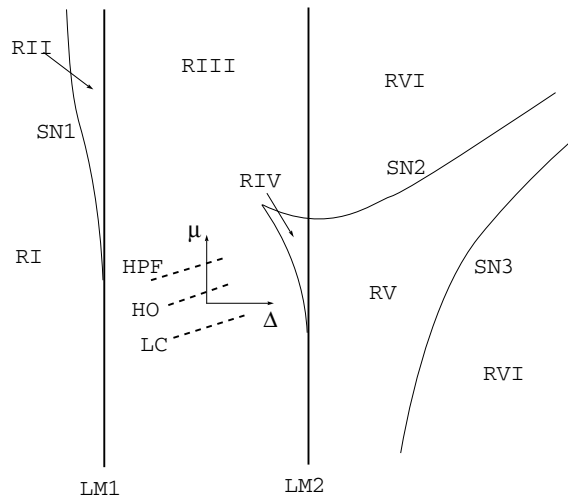
Fig. 6. Bifurcation curves for $A = 1$, $B = 3$, $\epsilon = 0.01$, $\alpha = \beta = \epsilon\mu$ as predicted by second-order averaging. The horizontal axis is Δ ($= \delta_1 + \epsilon\delta_2$) and the vertical axis is μ ($= \alpha_1 = \beta_1$) (see Table 1).

Table 1

Region	Total # fixed points	# Fixed points on $R = 0$	Curve	Bifurcation type
RI	0	0	LM1,LM2	Bifurcation of fixed points on $R = 0$
RII	2	0	SN1,SN2,SN3	Saddle-node bifurcation
RIII	3	2	HPF	Hopf bifurcation
RIV	5	2	HO	Heteroclinic bifurcation
RV	2	0	LC	Limit cycle created at ∞
RVI	0	0		

5. Bifurcations of periodic orbits in slow flow

Periodic orbits in the slow-flow equations correspond to quasi-periodic orbits in Eq. (1). In Eqs. (15) and (16), $R > 0$ and $-\pi/2 < \psi < \pi/2$ so that the phase space is $R^+ \times S^1$. There are two types of periodic orbits in Eqs. (15) and (16). We refer to *type 1* periodic orbits as those which plot as a topological circle in the R–ψ phase space and to *type 2* periodic orbits as those which are topologically equivalent to $R = $ const. Shown in Fig. 6 are dashed lines which represent bifurcations of periodic orbits in the simplified slow-flow Eqs. (15) and (16). The curve labeled HPF corresponds to a Hopf bifurcation in which a type 1 periodic orbit is born, HO corresponds to a heteroclinic bifurcation and LC corresponds to a type 2 periodic orbit being created. These bifurcation curves were found to exist by numerically integrating Eqs. (15) and (16) and observing the phase portraits generated.

Fig. 7 shows a sequence of phase portraits (R along the horizontal axis, ψ along the vertical axis) that were observed while holding δ_1 fixed and increasing μ in region RIII of the parameter space. Fig. 7(a) corresponds to being below the LC curve in region RIII where there exist only 2 saddle points on the $R = 0$ axis and an unstable fixed point with $R \neq 0$. As μ is increased, a stable type 2 limit cycle is observed to have been created as shown in Fig. 7(b) (darker trajectory). The creation of this limit cycle corresponds to the LC bifurcation curve. As μ further increases, the limit cycle moves in towards $R = 0$ until it eventually connects with the saddle points on the $R = 0$ axis forming a heteroclinic loop as shown in Fig. 7(c). This corresponds to the heteroclinic bifurcation curve HO. Increasing μ causes the previous type 2 limit cycle to become a type 1 limit cycle around an unstable fixed point (Fig. 7(d)). The limit cycle now shrinks around the fixed point it encircles until it disappears in a Hopf bifurcation changing the stability of the fixed point as shown in Fig. 7(e).
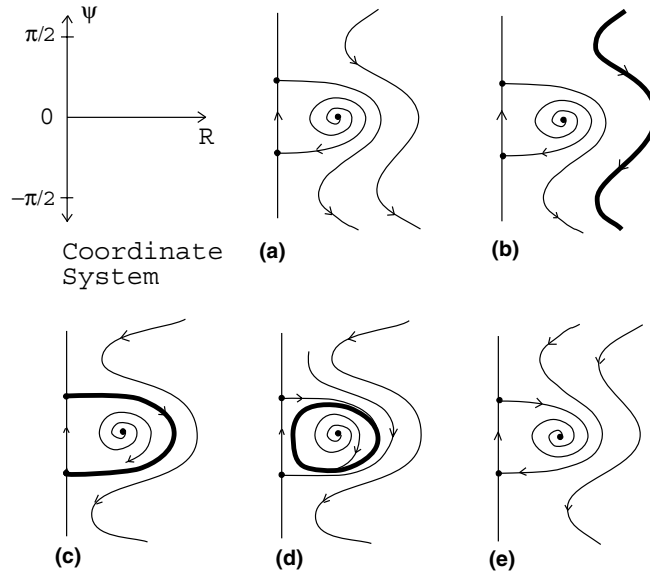
Fig. 7. Phase portaits of the sequence of bifurcations observed while holding δ_1 fixed and increasing μ in region RIII cf. Fig. 6.

6. Analysis using auto

The AUTO bifurcation and continuation software [1] was used to confirm the results previously obtained for the simplified system equations (15) and (16) and to investigate the bifurcation diagrams for different values of A and B in Eqs. (13) and (14).

The bifurcation diagram for Eqs. (15) and (16) generated using AUTO is shown in Fig. 8. It appears that the HPF and HO curves emanate from a common point $\mu = 0$ on the LM1 curve. In addition, both the HPF and HO curves exist
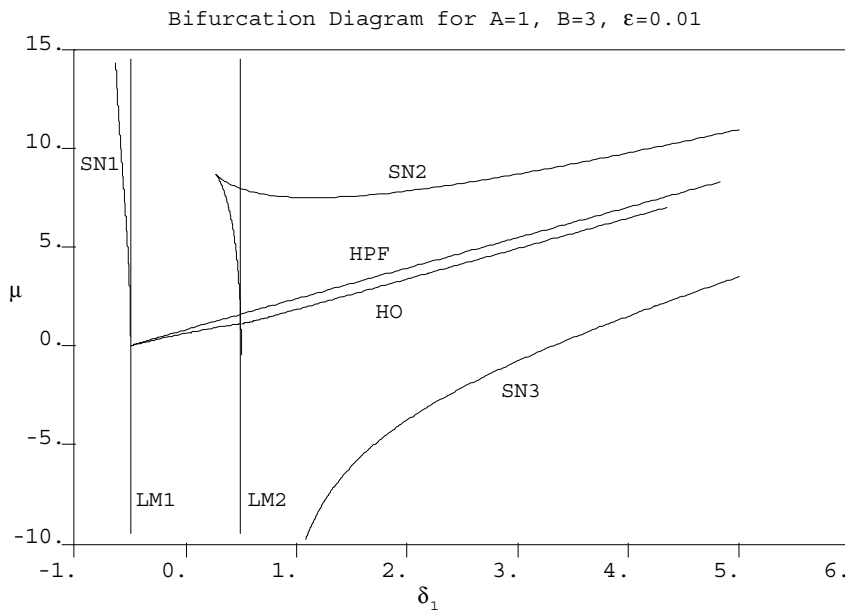
Fig. 8. Bifurcation diagram for $A = 1$, $B = 3$, $\epsilon = 0.01$, $\alpha = \beta = \epsilon\mu$ obtained by using AUTO to investigate the second-order averaging slow-flow Eqs. (15) and (16).

outside of the region bounded by the LM1, LM2 curves and continue into the region RV. AUTO has been used to obtain related bifurcation diagrams for various values of ϵ, A and B but these are omitted here for brevity.

7. Analytic approximation of Hopf bifurcation

At the point where the HPF, HO and LM1 curves intersect we have a degenerate bifurcation point ($\mu = 0$, $\delta_1 = -1/2$, $\delta_2 = -1/8$). An unfolding procedure outlined in ([2, Chapter 7]) was performed to investigate the dynamics around this point. We start by setting $\delta_1 = -1/2$ and introducing the following rescaling transformation:

$$R = \sigma\sqrt{u}, \quad \psi = \sigma v, \quad \mu = \sigma v_1, \quad \delta_2 = -1/8 + \sigma^2 v_2, \quad \tau = \epsilon\sigma t \qquad \text{for } \sigma \text{ small.} \tag{18}$$

Substituting Eqs. (18) into Eqs. (15) and (16) and Taylor expanding in σ, we get the following equations:

$$\frac{\mathrm{d}u}{\mathrm{d}\tau} = 2(1 + \epsilon)uv - \epsilon u^2\sigma - \left(2(v_1 - v)\epsilon u^2 + \frac{4}{3}(1 + \epsilon)uv^3\right)\sigma^2 - \epsilon u^2 v^2\sigma^3 + \mathrm{O}(\sigma^4), \tag{19}$$

$$\frac{\mathrm{d}v}{\mathrm{d}\tau} = v_2\epsilon - (1 + \epsilon)v^2 - \frac{\epsilon}{2}u + (v_1 + 2v)\epsilon u\sigma + \left(4\epsilon uv^2 - \frac{15}{8}\epsilon u^2 + \frac{1}{3}(1 + \epsilon)v^4\right)\sigma^2 - \frac{4}{3}\epsilon uv^3\sigma^3 + \mathrm{O}(\sigma^4). \tag{20}$$

A Hopf bifurcation occurs when the system has a pair of purely imaginary eigenvalues. We obtain a condition for Hopf bifurcations by requiring the trace of the Jacobian of Eqs. (19) and (20) be zero at the fixed point for which u is not zero. We start by first finding a series approximation for the fixed point:

$$u^* = u_0^* + u_1^*\sigma + u_2^*\sigma^2 + \cdots,$$
$$v^* = v_0^* + v_1^*\sigma + v_2^*\sigma^2 + \cdots, \tag{21}$$

where u_i^*, v_i^* are functions of ϵ, v_1 and v_2. We then substitute this solution into the Jacobian of Eqs. (19) and (20) and set its trace equal to 0. The condition that we find for a Hopf bifurcation to occur is:

$$v_1 = \frac{3\epsilon v_2\sigma}{1 + \epsilon} + \frac{9\epsilon(11\epsilon + 5)v_2^2\sigma^3}{2(1 + \epsilon)^2} + \mathrm{O}(\sigma^4). \tag{22}$$

Transforming back to the original parameters, we get the following approximation for the Hopf bifurcation curve:

$$\mu = \frac{3\epsilon(\delta_2 + 1/8)}{1 + \epsilon} + \frac{9\epsilon(11\epsilon + 5)(\delta_2 + 1/8)^2}{2(1 + \epsilon)^2}. \tag{23}$$

8. Limit cycle at infinity

Although we did not use AUTO to track the bifurcation curve associated with the creation of a type 2 limit cycle, we did find that the Hopf and heteroclinic bifurcation curves (HPF, HO) exist in region RV outside of the LM1, LM2 transition curves. For these bifurcation curves to exist, a type 2 limit cycle must have been created which suggests that the LC bifurcation curve should also exist in region RV and have a slope similar to the HPF, HO curves. This prompted the following analysis which results in an expression for the LC bifurcation curve.

In Section 5, we saw that a stable type 2 limit cycle was created somehow between Figs. 7(a) and (b), a result obtained by observing phase portraits of Eqs. (15) and (16) generated by numerical integration. Further investigation reveals that the type 2 limit cycle is created at $R = \infty$. Prior to the creation of the limit cycle, trajectories would escape off to $R = \infty$. This suggests investigating the behavior of the system for large R. Taking only the largest terms in R for Eqs. (13) and (14) with $\alpha_0 = \beta_0 = 0$ results in:

$$\frac{\mathrm{d}R}{\mathrm{d}t} = \epsilon^2\left(\frac{A}{2}\sin 2\psi + \frac{B}{12}\cos 2\psi + \frac{B}{2}\delta_1 - \beta_1\right)R^3, \tag{24}$$

$$\frac{\mathrm{d}\psi}{\mathrm{d}t} = \epsilon^2\left(-\frac{1}{24}B^2 - \frac{3}{2}A^2\right)R^4. \tag{25}$$

This system turns out to be integrable giving the solution:

$$R(\psi) = \sqrt{\frac{2}{J_2}\left(\frac{B}{24}\sin 2\psi - \frac{A}{4}\cos 2\psi + J_1\psi\right)} + C_1, \tag{26}$$

where $J_1 = (1/2)B\delta_1 - \beta_1$, $J_2 = -(1/24)B^2 - (3/2)A^2$, and C_1 is a constant of integration.

Note that $J_2 \leqslant 0$ and $\mathrm{d}\psi/\mathrm{d}t \leqslant 0$ (from Eq. (25)) so we can conclude that ψ is always decreasing in time for large R. Using these facts and Eq. (26), we see that as $t \to \infty$,

$$R \sim \sqrt{\frac{2J_1\psi}{J_2}} \tag{27}$$

so that for $J_1 > 0$, $R \to \infty$ as $t \to \infty$ (for sufficiently large initial R).

Thus, the LC curve is given by $J_1 = 0$ or $\beta_1 = (1/2)B\delta_1$. Numerical integrations of Eqs. (15) and (16) appear to agree with this condition.

9. Conclusions

In this paper we have performed a bifurcation analysis of a Mathieu equation with cubic nonlinearities restricting our attention to parameter values near the 2:1 resonance. We found that using first-order averaging could not explain some of the features observed by numerical integration and it was necessary to extend the analysis to second-order averaging. A bifurcation diagram was found for the second-order slow-flow equations.

The AUTO bifurcation and continuation software was used to obtain numerical bifurcation diagrams.

Finally, we analytically investigated some of the bifurcations associated with periodic orbits in the slow-flow equations.

Acknowledgements

References

[1] Doedel E, Champneys A, Fairgrieve T, Kuznetsov Y, Sandstede B, Wang X, AUTO 97: Continuation and Bifurcation Software for Ordinary Differential Equations. 1998.
[2] Guckenheimer J, Holmes P. Nonlinear oscillators dynamical systems and bifurcations of vector fields. Berlin: Springer; 1983.
[3] Nayfeh AH, Mook DT. Nonlinear oscillations. New York: Wiley; 1979.
[4] Rand RH. Topics in nonlinear dynamics with computer algebra. London: Gordon and Breach; 1994.
[5] Rand RH, Ramani DV, Keith WL, Cipolla KM. Theoretical study of a submarine towed-array lifting device. In: Tzou H, Golnaraghi M, Radcliffe C, editors. Proceedings of the 2000 ASME International Mechanical Engineering Congress and Exposition, November 5–10, 2000, Orlando, FL. Control of Vibration and Noise: New Millenium, AD-Vol. 61. New York: ASME; 2000. p. 39–50.
[6] Sanders JA, Verhulst F. Averaging methods in nonlinear dynamical systems. Berlin: Springer; 1985.